ÉCOLE POLYTECHNIQUE
FÉDÉRALE DE LAUSANNE

Master project in Physics

Length-dependent costs on optimisation problems with long-range connections

Carried out in the laboratory of Biophysics and Evolutionary Dynamics
in California, University of California Berkeley
Under the supervision of Professor Oskar Hallatschek

Done by

TOM SUTER

Under the direction of
Prof. Matthieu Wyart (advising Prof EPFL)
In the laboratory of Physics of complex systems

EPFL

Berkeley, August 23, 2018

Abstract

Here, we characterise the speed of spreading driven by dispersal events whose jump distances are broadly distributed but undergo some length dependant constraint. Using lattice-based simulations and scaling arguments, we compare how the range of the dispersal kernel is affected. Many models are now describing spreading from plant dispersal to viruses in a computer network. A change is known to happen when stochasticity is introduced but such models rarely include the space travelled as a constraint. While it may not be relevant in computer network, in many problem such as epidemics and plant dispersal travelling plays an important role. We present two stochastic models for the spreading, one happening on a fixed network and another one more homogeneously in space and time. By using different functions to characterise the importance of the distances travelled or the length of the links, we show how different patterns can emerge. Assuming a controlled way to implement the cost, we present theoretical results supported by simulations, whether one wants to accelerate the spreading or to slow it down.

Acknowledgements

I would like to give a special thanks to professor Matthieu Wyart and professor Oskar Hallatschek for giving me this incredible opportunity. I would also like to express my sincere gratitude to Jayson Paulose whose guidance and support have been a constant source of encouragement.

Contents

1 Introduction

About 4 billions years ago, life started its take over the planet. Evolutionary pressure brought us the current phylogenetic Tree. Survival of the fittest and mutations have constantly changed the living beings on earth. Since the beginning of Darwin's theory natural selection, we have been witnessed of increasingly fast discoveries. As we know we are reaching the golden age of datas, in biology it unfolds by the unraveling of the genetic code, result of the new accessibility of gene sequencing. Many progresses have been made, understanding genetic variation, cataloging the diversity of life, etc. But what mechanisms are important for large scale evolution and what set the time scales is very little known [1].

The propagation of a mutation in a population, the spread of a disease, animals and vegetal dispersal can be mathematically approached with similar models. They have a particular importance nowadays with large population widely interacting through efficient transport mechanisms across many scales [2, 3]. In this context, identifying and controlling the different regimes of the process becomes an important task. As we can imagine by the extent of application of this area of research, it is in the intersection of various fields, from ecology, population genetics to biology and statistical physics. One could wonder why statistical physics ? A necessary notion to understand it, is the fitness: the reproductive success of individuals with a specific genotype in a gene pool. Fitness landscapes which analyse the fitness as a function of gene change are often compared to energy landscape, well studied by physicists. For examples of many other similarities we recommend [4, 1]. We should mention that there is one aspect that may keep the two apart: in physics, when the number of constituents is large, thermodynamics focuses on average quantities and small fluctuations around these averages whereas rare events are essential in evolutionary dynamic. Furthermore, only a small step exist between spreading dynamic and networks. As we will see it is natural to map the individuals and the spread to networks which are another part of the physician toolbox.

Traditional approaches to address those problems tend to use deterministic approximations of the underlying stochastic process. There is an assumption that over many repeats of an event with a random element the stochasticity will average out, and can be ignored without invalidating results. Such models can often be analysed mathematically, but are sometimes sufficiently complex that a computational solution is necessary. The counterpart is that they predict under many conditions that spreading occurs at a finite constant velocity, [3].

The first derivation of the speed of invasion has been derived independently, the same year, by [5] and [6], from the equation known as the FKPP equation:

$$\frac{\partial n}{\partial t} = D\frac{\partial^2 n}{\partial x^2} + F(v) \tag{1}$$

which is, simply stating, a diffusion equation with a additional term counting for the growth of the quantity of matter, with D is a diffusion coefficient analogous to that used in physics. When $F(v) = An(1 - \frac{n}{K})$ the equation a "wave of advance" occurs as a well defined solution, more function described in. It asymptotically approaches the speed:

$$v = 2\sqrt{AD}$$

This diffusion coefficient describes the mean square distance over which a particle diffuses, and account for the "stochasticity" of the model. However, the use of a single parameter supposes that the dispersal kernel has tails bounded by an exponential, from arguments based on central limit theorem, which leads to this constant wave speed. This might be appropriate to some species but for some others rare long distance migrations are important [7]. When long-distance dispersal occurs either on a fixed network or more homogeneously in space, drastic changes occur [2, 8, 9]. The spreading becomes faster by seeding individuals around the initial cluster. The seeded satellites can then grow freely in their intact neighbourhood. The extent and rarity of the satellites depend on the kernel's tail, giving regimes from linear to exponential growth.

We show that when a restrictive function is added on top of the kernel, it helps limiting the propagation of the mutation in a controlled way. The problem naturally appeared when jumps have a "travel time". As a natural extension to previous models, we consider a period of time when the sent individuals are travelling and are not represented in any point of the space. Looking more carefully at the framework behind the problem, we show that this additional cost can be interpreted in a more general sense as a second resource to be optimized. For example, it can represent money needed for the jump to happen. We show that it can be interpreted as an optimization problem, well suited for transportations networks. A wide body of work showed how long range connections are changing the transportation network [10, 11, 12], and how different costs can affect it [13].

Using a power-law cost function, we present analytical derivations to predict the expansion of the outbreak at anytime. Findings go through convex cost, for which the growth becomes linear and concave cost where a faster than linear growth can be maintain.

2 Theory

2.1 Mathematical Modelling

We consider a lattice, discretisation of space, where each site is a "local area filled with a well-mixed population" called a deme. We consider then mutation occurring in every individuals at a rate u per generation. This type of dynamics is well know and modelled as following: The deme is fixed to size $\hat{n}$ with density $\hat{\rho}$ due to local resources. Mutant, appearing with rate u, take over the local population with a probability 2s. (They have a selective advantage over the original population.) The local population is considered well mixed, the number of mutants follows a logistic growth, detailed calculations are presented in section A.1:

$$\frac{dp_{mut}}{dt} = \alpha(1+s)p_{mut}\frac{\hat{n} - p_{mut}}{\hat{n}}$$

In evolutionary dynamics and population genetic, the different time scales are a major tool to simplify and understand the problem in a simple way. Here the variables characterising this evolution are:

- u: rate of mutation : mutation/(individual and generation)
- s: rate of colonisation of a deme (rate for an established mutation to fix in the entire pop)
- m: rate of migration (jump)

We assume that the local sweeps in a deme are fast compared to migrations. We can then ignore the logistic growth process within demes, so that when jumps occur and establish a new mutant population, it is saturated in the new deme by the next time step. Time is measured in units of the expected interval $(2s\hat{n}m)^{-1}$ between successive dispersal events per deme. We explain in the following section how jumps from a deme to another happens.

While the notion of deme is relevant when thinking of a mutation spreading through a microbial population, it is simpler to think of single individual in the case of disease or rumour spreading. For the sake of simplicity, in the following we will call the mutated demes "infected sites" and the wild type by "susceptible sites".

2.2 Dispersal Kernel

Starting with a single infected site in the lattice presented before, we allow the infection to travel to other site through a "jump" kernel. For every infected site, an event happens accordingly to a Poisson process of rate 1. An event englobes: drawing a distance $r \sim J(r)$ and setting the site, distant of r from the source, to infected. This whole process is equivalent to assign waiting times (t_{mn}) to all pairs (m, n) on the lattice, each of which is a random variable drawn from an exponential distribution with average time $1/J(r_{mn})$.

The extent of the outbreak is related to an optimization problem of finding the first passage times given this set of waiting times on the lattice.

Concerning the choice of the kernel, we know that any function bounded by an exponential can be modelled through the diffusivity in Eq. 1. We are thus interested by fat tailed distribution function. First they are needed to describe some species invasion [14] and secondly they tend to capture a really important phenomena present in networks, called small-world effect [9] and present in the humans social network [15].

Our models are discrete in space, and the probability of dispersal between sites x and y, over a distance r = x-y, is

$$J(|r|) \sim f(|r|), \qquad r \in \mathbb{Z}, r \neq 0 \tag{2}$$

To represent kernels incorporating long-distance dispersal, we will focus on one type of function leading to Lévy flights.

$$J(\vec{r}) \sim \frac{1}{r^{d+\mu}} \tag{3}$$

This power-law kernel has been studied by [2] and [3] and offers different behaviour related to different ranges of values for μ, compared to d denoting the dimension. Furthermore most of the literature is focused on power-law distributions because these have special mathematical properties and can be produced by interesting endogenous processes like feedback loops, self-organization, network effects, etc [16].

We see that the function $J(r)$ diverges as $r \to 0$. In reality therefore, the distribution must deviate from the power-law form below some minimum value r_{min} but in the context of lattice based simulation we set r_{min} to 1, meaning all the $J(r)$ for $r < r_{min}$ will be 0. In the real world, deviations may occur for short-range behaviour, but are unlikely to impact long-time invasion behaviour. For this reason, we also expect that distortions to our dispersal kernels, due to the discrete lattice or constraining $J(r)|_{r<r_{min}} = 0$, to have minimal impact on qualitative system behaviour.

To define a probability distribution, we need to normalize $J(r)$. The probability of making a jump to a ring of size dr of distance r is given by $r^{d-1}J(r)dr$. The normalization is given by:

$$Z = \int_{r_{min}}^{\infty} \frac{1}{r^{\mu+1}} dr = \frac{1}{\mu} r_{min}^{\mu} \tag{4}$$

We have the following probability distribution, $J(r) = \frac{1}{Z} r^{-(\mu+d)}$, having the following moments:

$$\begin{array}{rcl} < r^m > & = & \frac{1}{Z} \int\limits_{r_{min}}^{\infty} r^m J(r) \\ & = & (\mu + d - 1) r_{min}^{\mu} \cdot r^{m-(\mu+d)+1}|_{r_{min}}^{\infty} \\ & \sim & r_{min}^{m} \frac{\mu}{\mu+d-1-m} + \infty^{m-\mu-d+1} \end{array} \tag{5}$$

defined when $m < d + \mu - 1$. In dimension 1, for $\mu \leqslant 1$, the mean diverges. In that case for finite sample size, the mean is dominated by the largest value. For $1 < \mu < 2$ the mean is finite and the the variance diverges.

2.3 Standard Models

Following the procedure of [2], we will introduce the concepts required to derive the analytical results. The goal being to characterise the extent of the infected population at any time, we need to know the speed at which it will grow. To do so, we use the characteristic linear size $\ell(t)$ - loosely the radius of the core of infected population. For long time we have : #infected sites $\approx \text{area}_d \cdot \ell^d(t)$.

When working with mutation and the rates defined in section 2.1, it is convenient to define the probability of jump together with probability of that mutant establishes times the density :

$$G(r) = s\hat{\rho}J(r) \tag{6}$$

$d^dxd^dyG(|\vec{x}-\vec{y}|)$ is the rate at which a saturated mutant population near $\vec{x}$ generates a mutant pop at $\vec{y}$. In light of those settings, we see that at the deme level new mutation fix within wild type demes at the rate $2s\hat{n}u$ and mutated demes send migrants at rate $2s\hat{n}m$. Therefore we measure time in units of the expected interval between successive dispersal attempts per deme: $\frac{1}{2s\hat{n}m}$. It means that in that fraction of a generation we have a successful migration coming out of the deme.

In this context, the core region $\ell(T)$, grows by incorporating sub-outbreaks at time T, which have migrated at earlier time, Fig. 1b. The condition of having, on average, about one jump from source to target region can be stated mathematically as

$$\int\limits_0^T dt \int\limits_{B(\ell(t))} d^dx \int\limits_{B(\ell(T-t))} d^dyG(|\ell(T)\vec{e}+\vec{y}-\vec{x}|) \sim 1 \tag{7}$$

This recurrent relation relates the evolution of seeded cluster to the core radius. From a geometric argument, we see that the seeded satellites need to start in the inverted funnel to contribute to the core at time T, Fig. 1a. Using G defined above and large enough r such that small satellites are negligible compared to the core radius, one can derive asymptotic results of $\ell(t)$ for the spectrum of μ.

If the growth rule is much faster than linear the significant contributions to the integral arise from source and target regions of size much smaller than $\ell(T)$, which leads to:

$$G[\ell(T)]\int\limits_0^T dt\ell^d(t)\ell^d(T-t) \sim 1 \tag{8}$$

If ℓ(T) grows faster than linearly but slower than exponentially, the integrand develops a peak at $t = T/2$. A saddle-point approximation can then be used to obtain the even simpler expression:

$$TG[\ell(T)]\ell\left(\frac{T}{2}\right)^{2d} \sim 1 \tag{9}$$

This expression has an analytical solution, using $\log_2(\ell(t)) = \ \phi(z)$, derived in Appendix A.2.

$$\phi(z) \approx \frac{z}{\mu-d} + \frac{2d}{(\mu-d)^2}\left[\left(\frac{2d}{\mu+d}\right)^z - 1\right] \tag{10}$$

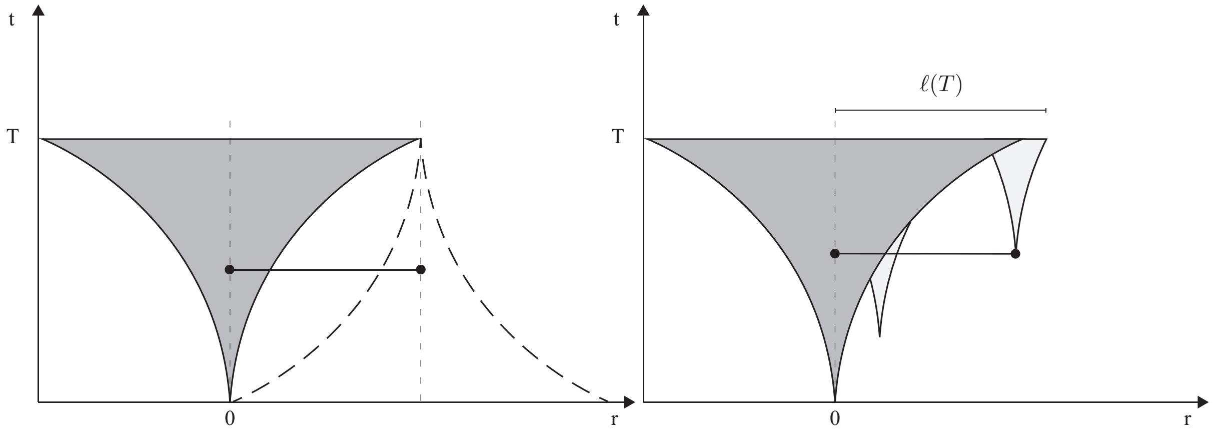

(a) Inverted funnel in dashed lines with approximation for the key jump at time $\frac{T}{2}$

(b) Growth of the core funnel by incorporation of small seeded clusters

Figure 1: Funnel picture

It leads to the following behaviour:

- When $d < \mu < d+1$: the first term of Eq. 10 dominates at large z and we have (using $\phi(z) = \log_2(\ell(t))$) : $\ell(t) \sim A_\mu (ct)^{\frac{1}{\mu-d}}$
- When $\mu < d$: the second term dominates at large z due to the exponential growth and we have : $\ell(t) \sim \exp(B_\mu t^\eta)$ with $\eta = \log_2(\frac{2d}{\mu+d})$
- When $\mu = d$: both therms needs to be accounted, furthermore we can show that the result: $\ell(t) \sim \exp(\frac{\log^2(t)}{4d\log(2)})$ is valid not only for asymptotic behaviour but also intermediate regime, [2].

We shall now introduce the basis of the second model. We consider the spreading on a fixed network. Each site is considered as a node with a fixed number of links k_i with probability of a connection $J(r)$, between each pair of sites distant by r. This algorithm simulates an SIR epidemic with an active period of one step per site. When k is constant, it is equivalent to 'model A' of Grassberger [17, 18]. Results have been derived by [2] and [19], and introduced in section A.3. The asymptotical functions have the following forms:

- When $d < \mu < d+1$: $\ell(s) \sim s$
- When $\mu = d$: $\ell(s) \sim s^\nu$
- when $\mu < d$: $\ell(s) \sim \exp(c_2 B_\mu t^\eta)$

2.4 Length-Dependent additional cost

2.4.1 Basis

One shortcoming of the model is that it assumes instantaneous jumps or similarly that all links have the same cost. In reality, jumps could take some time that depends on the distance. For the ecological problem, in which the time between jumps is measured in generations, this is probably less relevant: the rates are to be interpreted as probabilities that jumps occur over certain distances between generations, whereas the dispersal itself happens over short times compared to the generation time. However, for general optimization problems such as optimal transportation protocols, the travel time itself might be an important contribution to the cost associated with getting from point A to point B.

The generalized problem can be expressed in optimisation language. Now, instead of minimizing the sum of waiting times, we need to minimize the sum of waiting times and cost of the corresponding jumps, adding a deterministic part to the stochastic one.

$$\tau[\mathscr{P}] \equiv \sum_{i=1}^{s} t_{j_i,j_{i-1}} + C(r_{j_i,j_{i-1}}). \tag{11}$$

In the following we will call this sum on a path the "netcost". The "Outbreak" algorithm presented in next section propose a way to numerically solve such problems minimizing computational efforts.

The funnel picture capturing the iterative argument for jump-driven growth can be modified in the presence of generalized cost functions by considering the evolution of the growth funnel in space and generalized time. The source-target picture is preserved, provided the netcost is represented on the vertical axis. If we define $\ell(\mathcal{T})$ as the extent of the region which can be reached such that the optimal total cost is $\tau < \mathcal{T}$, then a similar iterative argument constrains this function: the total number of jumps leading to an outbreak which merges with the core at $\mathcal{T}$ should be of order 1. However, this key jump is no longer horizontal on the $(\mathbf{x}, \tau)$ plane but instead lands at a value of τ that is higher than the source by the additional cost $C[\ell(\mathcal{T})] \equiv C_{\mathcal{T}}$. Assuming that the source and target areas are still small compared to $\ell(\mathcal{T})$ (i.e. growth is still faster-than-linear), the consistency Eq. 42 is modified to:

$$G[\ell(\mathcal{T})] \int_0^{\mathcal{T}-C_{\mathcal{T}}} d\tau\, \ell^d(\tau)\ell^d(T-\tau-C_{\mathcal{T}}) \sim 1$$

and the saddle point approximation to:

$$\frac{\tau - C_\tau}{2} G[\ell(\tau)]\ell^{2d}(\frac{\tau - C_\tau}{2}) \sim 1 \tag{12}$$

An important feature used to derive Eq. 9 was that the time symmetry of the source and target, due to the instantaneous jumps, related the funnel size at T to that at $T/2$. Imposing a time for the jump will break the symmetry and the integral in Eq. 12 will be dominated by contributions at $\tau = (\mathcal{T} - C[\ell(\mathcal{T})])/2$.

Even-though Eq. 12 is not easily approach, some graphical intuitions give us sufficient information to predict the behaviour.

2.4.2 Generalized cost forms

Every action, every movement has a price. While it may be negligible in some cases, most of the time the energy, money or time involved affect greatly the action. Cost occurs even in plant dispersal [20] and animals. For example among birds, short-flight are more costly than steady-state flights [21] whereas in land animals it tends to be more linear [22]. For humans the different transportation systems offer different range of prices per kilometre. It might be more of a concave function switching from car to train or convex when switching from train to plane, [23].

Facing such diverse type of cost, we aim for a framework giving us the more flexibility. In the following we used a power-law: $C(r) = Ar^{\beta}$ which is relatively simple, can be tuned through β to give three different regimes: concave, linear and convex. We expect that the behaviour resulting from complicated function such as Log can be approximate by some convex power law. We put away exponentials decay and other strongly decaying functions as they seem less present in studied systems and secondly they would only affect the growth for a short period of time.

We presented first the cost as an travel time. In order to be one, $C(r) = Ar^{\beta}$ must have time unit, meaning A must have units: [time/distance$^{\beta}$]. Depending on the problem at hand, A might have other unit to represent the correct quantity.

3 Implementation

A problem that arises when simulating stochastic processes is actually drawing the random variable, [24]. A simple and preferred method (when available) is the inverse method. Inversing the cumulative distribution of the powerlaw allow us to use a uniform sampler available on most programmation languages.

3.1 Outbreak

The numerical implementation of the modelling presented above requires some specific containers in order to optimally access, and sort the data. The goal is to be able to simulate large systems size, $\sim 10^7$ demes, as fast as possible.

We begin by setting the initial conditions, the lattice is initialised with one infected site at time $t = 1$ and position $[0]^d$. Each site is either infected or susceptible. We then proceed through a series of iterated steps that take place every timestep, $dt = \frac{1}{N}$, which are illustrated on the left panel of Fig. 2:

1. Time is updated to $t + dt$, an infected site is chosen randomly within the infected population and a spreading attempt to $r \sim J(r)$ is made with landing time: $C(r)+t$.
2. If the landing position is not already infected and the current landing time is bigger than $C(r)+t$, then the attempt is stored and current landing time to that destination changed to $C(r)+t$. Note that departure time as well as the source need to be stored for the computation of the jump time when cost is considered as external resource.
3. Land every stored attempts for which landing time $\leqslant$ t. For every such landing do: $N = N + 1$.
4. Steps 1 to 3 are repeated until the termination condition is met.

We see that every stored attempt requires four values: the departure time, the source, the landing time and the destination. The first two are needed to compute the actual time without cost at which each jump was done.

For optimal usage of this algorithm, specific containers should be used to store the infected sites. Random access to a position is needed as well as checking easily if a site is already in the list. One way, is to store the sites both in a vector which allows O(1) access at a random site and in a set to verify in O(ln(N)) if the site is already infected. The stored jumps waiting to be approved are stored in an ordered map which allow O(ln(N)) lookup for a better landing time and O(ln(N)) to find all the sites that should have landed at time t.

As the goal is to go to large system size, we do not impose boundaries on the lattice. The boundaries are fixed by the size of the container used: long int. It allows to have infected deme up to $9.223 \cdot 10^{18}$ on both side of the source. While being not too restrictive, and usually not too costly since only the infected sites and potential jumps are stored, it may lead to problem for very large kernels. In those cases, attempts far from the core radius will be more frequent and never actually used, but still stored and fill the memory. Specially using the STL library in C++, the values stored in unordered-set are know to take up to 10 times more memory per element stored, (a one byte value stored in a unordered set allocates around 10 bytes of memory) [25]. For example a lattice of 10^7 completely filled will require 800 Megabytes for a single double stored at each site of the lattice. But for $\mu < 1$ attempts can often fill more than 10 times the final size, and at least 4 values are need per site, leading to Gigabytes of memory. Therefore a cut off setting the maximum jump length accepted should be used in those cases.

The adaptive timestep and the random ensure that the jump events follow a Poisson distribution with rate 1. It will also assure that the waiting times from a source to destinations follow an Exponential distribution.

3.2 Tree

The Tree algorithm needs to meet the same requirements as before. We now use a slightly different version of cost, adding a constant term that accounts for the active period of each site: $C(r) = Ar^{\beta} + \delta$. The fixed number of outgoing links from each node and the absence of exponentially distributed waiting time make this model very different. A new algorithm more adapted is presented. We begin with similar initial conditions: the lattice is initialised with one infected site at position $[0]^d$, with $C_{parent} = 0$. Each site is either infected or susceptible. We then proceed through a series of iterated steps which are illustrated on the right panel of Fig. 2 :

1. Pick a source node with minimum cost in the list of waiting nodes, delete it from the list and if not in the population add it to it, otherwise redo step 1.

2. Add +1 at position [generation parent+1] in the vector tracking the number of nodes reached at each generations.

3. From the source node, send $(k_i - 2)$ offsprings to $(k_i - 2)$ distances r drawn in $J(r)$, and 2 sites to the direct neighbours.

4. For each attempts of jumps verify if the destination is not currently in the population and calculate the total cost to that node $C_{total} = C_{parent} + C(r)$, using $C(r) = Ar^{\beta} + \delta$.

5. Add the new jumps in the list of waiting nodes with the associated $C_{parent} = C_{total}$.

The more familiar with Dijkstra's minimum-path algorithm [26], will note that this reproduces the same procedure but builds the network on the fly and chooses only the optimal path. A convenient way to store the waiting nodes is in a min-heap sorted by total cost value, in such a way that the heap head will always have the minimum cost value. Using this container allow to extract the minimum (and delete it from the heap) in O(log(N)), and add new elements in the sorted heap in O(log(N)). Using this algorithm might lead in storing useless links, for example a new jump to destination j is added but a more costly one was already in the heap: they will both be stored in the heap. However it is faster to keep irrelevant links in the heap than looking for them an delete them.

Concerning the infected site, they are just store in a set since no random access is needed here.

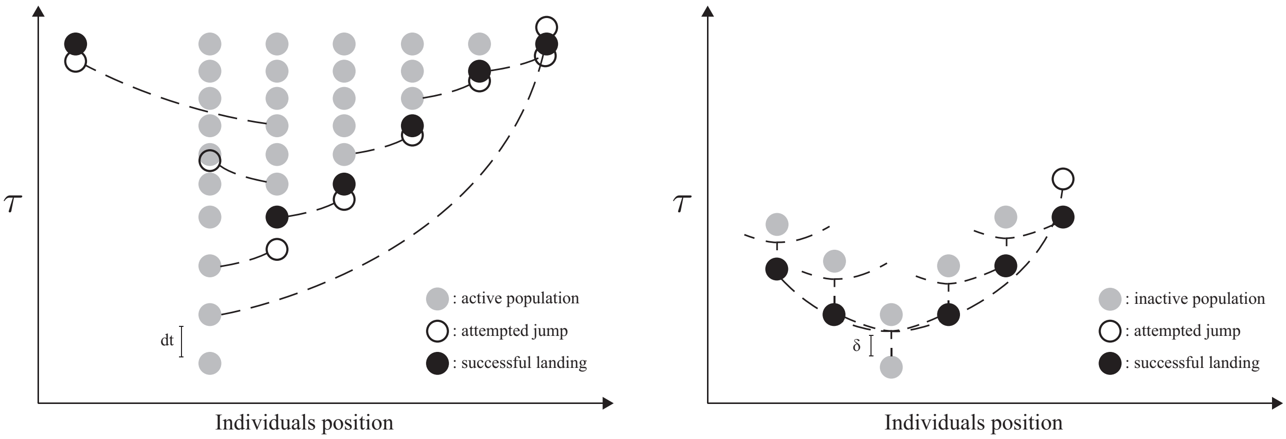

Figure 2: **Outbreak** and **Tree** Algorithms example with a convex cost. As netcost, τ, increases the first attempted jump for any positions at that τ is accepted and the later ones to that position are discarded. The set of small jumps in the **Outbreak** scheme is unlikely but represented here to illustrate that it can be more advantageous to do such a series than a long jump. In the **Tree** example with $k_i = 4$, we show show only one jump after the first generation, the three others are denoted by an unfinished line.

4 Results

The following table resumes all the parameters and names of variables used to describe and analyse the model. Some of the variables will be used later in the section.

Variable Name	Meaning
μ	jump distribution parameter
A	prefactor of the cost function $C(r) = Ar^{\beta}$
β	exponent of the cost function
τ	netcost in Outbreak and in Tree
t	time in Outbreak
s	steps in Tree
γ	subleading order of the growth in Outbreak
λ	subleading order of the growth in Tree
k_{out}	number of outgoing links from a node in Tree

Table 1: Description of frequently used variables

Concerning all the Results section, we draw the attention on the dimensionality. While we derived asymptotical behaviour for an arbitrary dimension only dimension 1 has been numerically analysed. With the mean of more computational resources it would be possible to simulate systems of dimension 2 where we expect similar behaviour.

4.1 Outbreak

To derive the behaviour with cost, we will assume that the bare growth is known and has the following form:

$$\ell_0(t) = \begin{cases} c_1[c_2(\mu+d-1)t]^{\frac{1}{\mu-d}}, & \text{if } \; d < \mu < d+1 \\ c_1\exp(\frac{c_2\log^2(t)}{4d\log(2)}), & \text{if } \; \mu = d \\ c_1\exp(c_2 B_\mu t^{\eta}), & \text{if } \; \mu < d \end{cases} \tag{13}$$

Where c_1 and c_2 are fitted values.

4.1.1 Convex Cost

We first analyse the case of strongly limiting functions. In order to do so, we come back to the key-jump argument. Analysing the evolution with the cost function added as an extra time: $\ell(\tau)$. When the growth follows its unperturbed expansion, the key jump extend over distances many times the size of the growth funnel at the time of the jump due to the non-linearity of the growth. The extra time of that jump, consequence of the cost, will lead the key jump landing into an already filled region, Fig. 3a. Long jumps cannot occur anymore and the growth is now limited to a linear mode where only small jumps can contribute to the growth. The extent to which we can expect a "normal" behaviour is given by the length jumps can have without landing into a filled part:

$$t^* \approx C[\ell_0(t^*)] \tag{14}$$

Jumps of size $r > \ell_0(t^*)$ will land on an occupied zone, and will not be part of the growth. We can expect that at this t^*, the $\ell(t)$ under cost has deviated from $\ell_0(t)$ because no seeded funnel could have been planted so far. $\ell(\tau)$ will eventually become linear when the core radius is a couple of times $\ell_0(t^*)$.

It reduces to a regime similar to deterministic models with here a speed depending on the cost. In that case we can analytically derive the speed after the transient acceleration. More precisely, we measured that $2 \cdot t^* \approx C[\ell_0(t^*)]$ is better fitted to derive the t^*, Fig. 4. We can interpret this reduced cost as following: after the growth deviates, it needs an extra time to reach a linear state during which the speed still increases. From t^*, the speed can be calculated assuming the linear curve intersects at $\ell_0(t^*)$ and starts at 0, Fig. 4. The slope of the curve is simply given by:

$$v_t = \frac{\ell_0(t^*)}{t^*} \tag{15}$$

This assumption matches the numerical results: if t^* in Eq. 15 is replaced by $t^*_{\text{numerical}}$ then $v_t = v_{t,\text{numerical}}$: the interpolated velocity from the measured intersection is exactly the measured velocity. An analysis for two values of β and a range of A is presented in Fig. 5a.

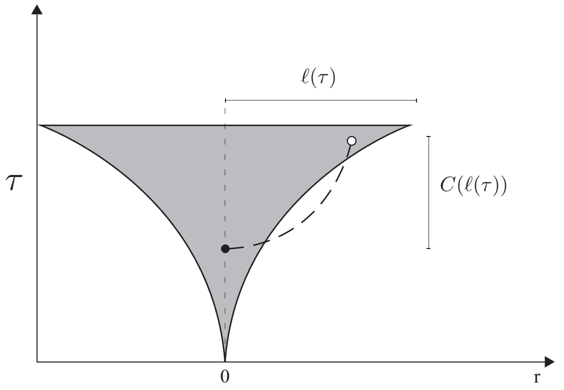

(a) Funnel picture with convex cost and a failed key jump

(b) Key jump starting on average at $t^*/2$, finishes at the end of the funnel.

Figure 3: Different cases of convex cost

For the cost as an additional time to pay, the netcost case, the cumulated traveling times slow the grows even more. Arriving at $\ell(t^*)$, they are scaling as $C(\ell_0(t^*))$. It leads to the τ^* equation:

$$\tau^* - C(\ell_0(\tau^*)) \approx C(\ell_0(\tau^*))$$

In other words, subtracting the expected jump times required to reach $\ell_0(\tau^*)$ allows to use the form ℓ_0 which supposes no jump time. The calcul of τ^* is represented in Fig. 4 showing detailed simulation of τ^* for a specific $C(r)$ and μ. t^* and $\tau*$ matches the numerical results.

We now see that both the more precise way of calculating t^* and τ^* are simply a rescaling of A. Let us consider Eq. 14 for a generic A and derive the values of t^* using Eq. 13.

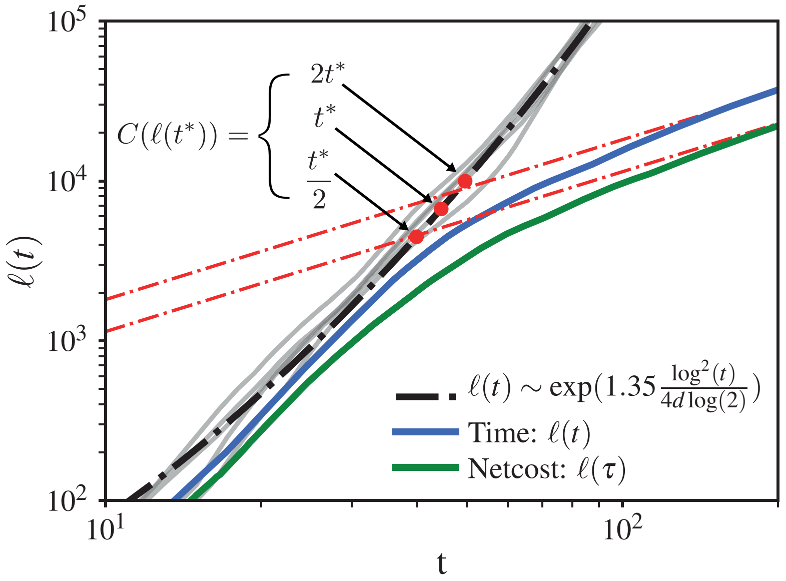

Figure 4: $\mu = 1$ **and additional cost** $C(r) = 10^{-6}r^2$**:** Growth in time (blue) and netcost (green) with respective fitted asymptotical linear form in red. The dots are calculated from the presented equation while numerical solutions can be derived finding the intersection between the red fits and the black fit.

$$t^* = \begin{cases} \left(Ac_1^{\beta}((\mu - d + 1)c_2)^{\frac{d\beta}{\mu - d}}\right)^{\frac{1}{1-\beta d/(\mu-d)}}, & \text{if } d < \mu < d+1 \\ \exp[(1 + \sqrt{1 - \frac{c_2 \cdot \log(Ac_1^{\beta})}{\log(2)\beta}}) \cdot \frac{2d\log(2)}{c_2\beta}], & \text{if } \mu = d \\ -W\left[-(Ac_1^{\beta})^{\eta} \cdot \eta c_2 \beta B_{\mu}\right]/(c_2\beta B_{\mu}\eta)^{1/\eta}, & \text{if } \mu < d \end{cases} \tag{16}$$

We can then derive v_t as a function of β and A leaving implicitly the μ dependance in t^*:

$$v_t = \frac{\ell_0(t^*)}{t^*} = \frac{A^{-1/\beta}t_*^{1/\beta}}{t^*} = \frac{t_*^{\frac{1}{\beta}-1}}{A^{1/\beta}} \tag{17}$$

On Fig. 5 we can see the calculated speeds from Eq. 17 compared to simulated ones for both netcost and time. The predictions agrees with simulations for a wide range of dispersal kernels and cost functions with an impressive precision. The incertitude on the derived speed is only coming from the fitted values c_1 and c_2 used in ℓ_0 not relevant here. The limitation of the fitted dots happens when the cost gets lower ($A \downarrow$ and $\beta \downarrow$), longer and longer simulations are needed to see where the restricted growth leaves ℓ_0 leading to a wrong fit when the crossover size is not reached. High values of A have not been analysed here as they fall into a case that depends on the specificity of the lattice. The case is discussed in section A.4.

Before going further, an additional remark should be said when $\beta = 1$, results in netcost are similar to the ones for $\beta > 1$. Indeed the same principle is valid: the jump cannot go faster than linear speed which sets the type of growth, as shown on Fig. 3a.

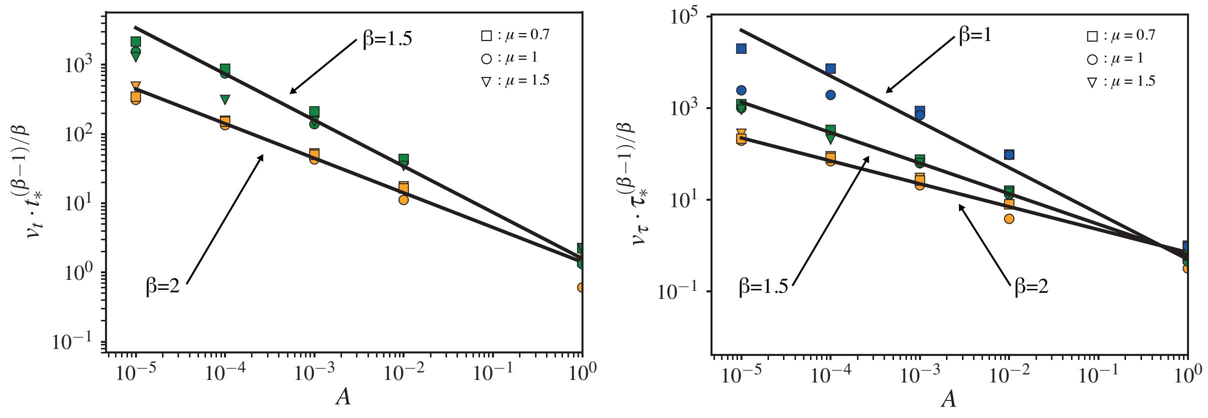

(a) time speed

(b) netcost speed

Figure 5: **Rescaled speed for Outbreak case**: The geometric forms are the fitted speeds put into the rescaled form Eq. 17, using t^*_{sim}: the intersection of the fit and ℓ_0

Furthermore we will see that it coincides with the behaviour for concave cost in the limit $\beta \to 1$. However when we consider time framework, β curves are faster than linear as we expect in the limit of concave cost, section 4.1.2.

4.1.2 Concave Cost

Let us consider $C(r) \sim r^\beta$ with $\beta \leq 1$ (i.e. concave down, so that the cost per distance falls with distance). We ask ourselves how fast can the spread infect the lattice.

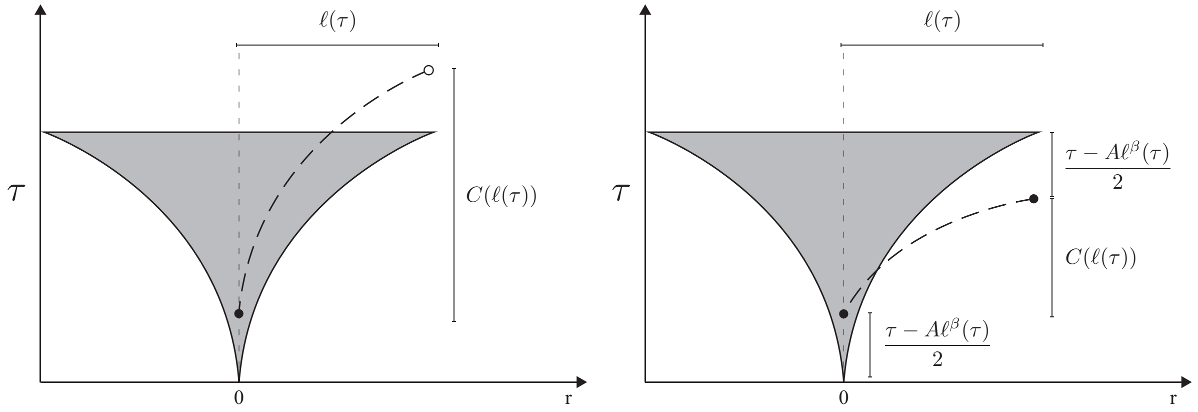

$\ell(\tau)$
τ
$C(\ell(\tau))$
0
r
$\ell(\tau)$
τ
$\frac{\tau - A\ell^\beta(\tau)}{2}$
$C(\ell(\tau))$
$\frac{\tau - A\ell^\beta(\tau)}{2}$
0
r

(a) Funnel picture with concave cost and a failed key jump

(b) Funnel picture with concave cost and successful key jump

Figure 6: Graphical intuition for failed and succeeded jumps

We consider jumps taking $C(r)$ time to travel. At long times, this requires that the funnel growth with τ can be no faster than $\sim \tau^{1/\beta}$, because otherwise the key jumps would eventually land in a region that is already occupied, Fig. 6a. Similarly to the convex case, we aim to find at what point the cost becomes relevant. We expect that it happens at τ^* such that $C(\ell_0(\tau^*)) \sim \tau^*$, after that time, key jump would be limited by the cost function and the growth would slow down. However, it might never happen. Indeed ℓ_0 grows faster than $\tau^{1/\beta}$ therefore $C(\ell_0(\tau^*))$ grows faster than τ. In such cases we argue that the cost is always limiting Fig. 6a, but by reducing A we can reach regimes where the two functions intersect.

Analysing that intersection on simulation, we see that it is not sufficient to give a good scaling on when the cost saturates the growth. The intersection occurs orders of magnitude before any noticeable change. We propose a way to certify when A is high enough but we remain unable to answer the "when" question for an arbitrary cost.

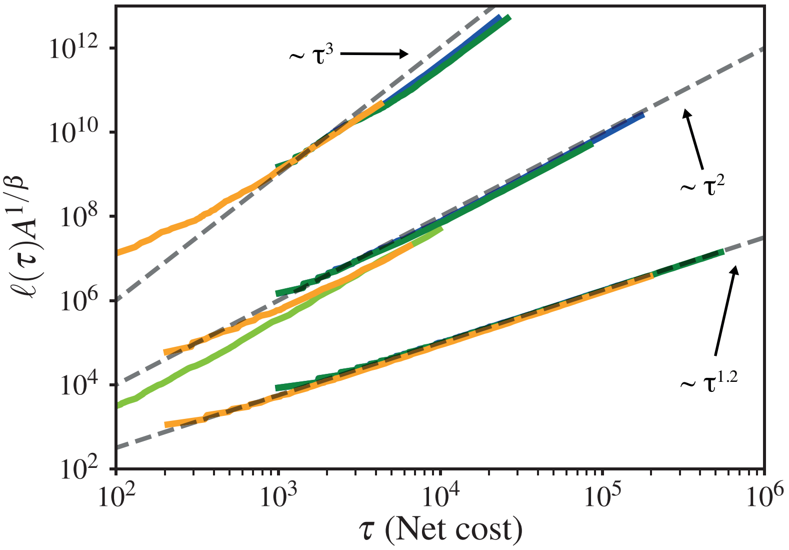

Figure 7: **Rescaled growth for various concave cost and μ.** The grey curves represent the asymptotical growth expected for the three β (0.33, 0.5, 0.8) used with a constant speed. All $\ell(\tau)$ have been multiplied by $A^{1/\beta}$ which correspond to the inverse of the speed. For each β we plotted three values of μ. Orange: $\mu = 1.3$ and $A = 2 \cdot 10^2$, Green/light Green : $\mu = 1$ and $A = 10^3/A = 10$, Blue: $\mu = 0.7$ and $A = 10^3$

We recall that ℓ_0 has different form depending on μ. We expect a qualitative change for $\mu \leqslant d$, the marginal and stretched-exponential cases are, always growing faster than what can be supported by the cost function. However in the power-law growth regime, Eq. 13, when $d < \mu < d+1$, the growth may be maintained if $\frac{1}{\mu - d} < \frac{1}{\beta}$, the long time functional form can remain unchanged.

We present different scalings of growth on Fig. 7 associated with β values for different μ. It is interesting to note how the speed becomes constant across all values of μ. When the cost is limiting and the asymptotical regime reached, the growth is driven by the long jumps which are limited by $\ell(\tau) = v_\tau \tau^{1/\beta}$:

$$C(\ell(\tau)) = C(v_\tau \tau^{1/\beta}) = \tau \tag{18}$$

It follows that $v_\tau = A^{-1/\beta}$. The constant speed across different values of μ can be seen on Fig. 7. The speed becomes independent of ℓ_0 and therefore μ. The cost will transform any functional growing faster than $v_\tau \tau^{\frac{1}{\beta}}$, to that form. The light green curve should be compared to the darker green which both have similar parameters but different A.

For lower values of A, the crossover is at later times. It follows naturally by an increased velocity. The only impact of μ is to change the timescale at which the cost is relevant for a given A. As mentioned, when $\frac{1}{\mu-d} < \frac{1}{\beta}$, the previous arguments do not apply and we can see that when μ gets closer to the limiting case the behaviour is less precise, Fig. 7.

We now analyse more deeply the τ dependance in that case. We start by looking at the saddle-point approximation in Eq. 12:

$$\ell^{d+\mu}(\tau) \sim [\tau - A\ell^{\beta}(\tau)]\ell^{2d}\left(\frac{\tau - A\ell^{\beta}(\tau)}{2}\right) \tag{19}$$

Now assuming $[\tau - A\ell^{\beta}(\tau)] \sim \tau$ (we recall that $\ell(\tau) \sim \tau^{1/\beta}$), and putting it in Eq. 19 :

$$\tau^{\frac{d+\mu}{\beta}} \sim \tau \cdot \tau^{\frac{2d}{\beta}}$$

In order to be valid we need to impose: $\mu = d + \beta$. The only assumption we had for $\ell(\tau) \sim \tau^{1/\beta}$ was: $1 > \beta > \mu - d$ when $\mu > d$, and all $\beta > 0$ when $\mu \leq d$. Clearly it includes a wider range of parameters, $\frac{1}{\beta}$ cannot be the full dependence but only the leading-order one. Otherwise the scaling $\ell(\tau) \sim \tau^{1/\beta}$ would be valid only for $\mu = d + \beta$. The natural form for the first subleading term to the power law is also a power law, anything faster is excluded, and if anything slower had a natural scale e.g. exponential, then at long times the area of the source and target regions would shrink to 0. For the balance of Eq. 19 to yield a power law across ever-growing values of total cost, we can set:

$$\tau - A\ell^{\beta}(\tau) \sim \tau^{\gamma},$$

i.e. the first correction to the leading behaviour due to the key jump at net cost τ scales as τ^{γ}, with the requirement that $\gamma < 1$. Putting this form into Eq. 19, and using $\ell(\tau) \sim (\frac{\tau-\tau^{\gamma}}{A})^{1/\beta}$, we see that:

$$(\frac{\tau - \tau^{\gamma}}{A})^{\frac{d+\mu}{\beta}} \sim \tau^{\gamma}(\frac{\tau^{\gamma} - \tau^{\gamma^2}}{A})^{\frac{2d}{\beta}}$$

For the he leading terms to match, we must have the scaling:

$$\gamma = \frac{\mu + d}{2d + \beta}, \tag{20}$$

which indeed satisfies $\gamma < 1$ in the case when growth is cost-limited ($1 > \beta > \mu - d$ when $\mu > d$, and all $\beta > 0$ when $\mu \leq d$).

Looking at a some simulations at the opposite side of the spectrum of γ, Fig. 8, $C(\ell(\tau))$ does appear to follow τ, meaning $\ell(\tau) \sim \tau^{\frac{1}{\beta}}$, with a systematic deviation, scaling as τ^{γ}. As we increase A for the same parameters, the asymptotical behaviours can be reached for same final size but at a later netcost, see bottom panels Fig. 8. We can now use this subleading term to estimate the expected growth in waiting time. First let's write the netcost τ as a function of ℓ:

$$\tau(\ell) \approx A\ell^{\beta} + c\ell^{\beta\gamma} \tag{21}$$

The first term is the contribution from the net cost of the key jump which has length of order ℓ, whereas the second term encompasses the contribution from the source and target "feeder" funnels (see Fig. 6b).

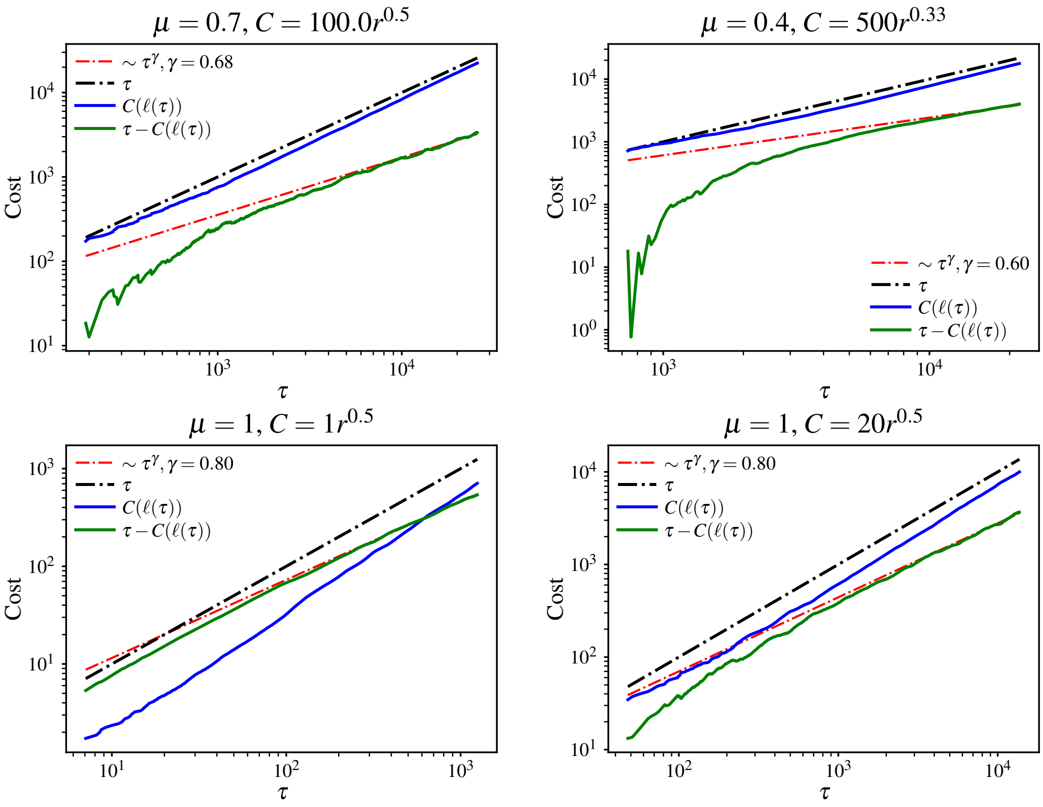

Figure 8: **Leading and subleading contributions to net cost**, $\beta = 1/2$ from simulations (solid lines) compared to power-law predictions (broken lines). The prediction for γ is given in Eq. 20. The plot are averaged over 4 simulations or more of final size: $\ell(\mathcal{T}) = 5 \cdot 10^5$.

This result gives us an upper bound on the scaling of the waiting times t. We recall that τ includes the sum of the waiting time, t, for a path up to $\ell(\tau)$ and the sum of the costs in that path. Since we are considering a concave cost we know that $\sum_{i=source}^{n} C(r_i) \geqslant A\ell^{\beta}$, it leaves us with $t \leqslant c\ell^{\beta\gamma}$. Now a second limit can be derive using the key jump argument. If we look at the funnel picture in waiting time, and consider the extent $\ell(\tau)$, we know that there must be some time t during which the core radius sends one seed. $\ell(\tau)$ being the size at the end of the key jump, it is overestimating the size of the source to use during t. The key jump equation in waiting time is similar to Eq. 19,

$$\ell(\tau^{\gamma})^{2d}\ell(\tau)^{-\mu-d}t \geqslant 1 \tag{22}$$

Now replacing $\ell(\tau)$ by the leading order $\tau^{1/\beta}$ we have: $t \geqslant \tau^{(\mu+d-2d\gamma)/\beta} = \tau^{\gamma}$ and finally going back to $\tau \sim \ell^{\beta}$, we have: $\ell(t)^{\gamma\beta} \leqslant t$.

In the light of the bounds on t, we expect $\ell(t) \sim t^{\frac{1}{\gamma\beta}}$. The exponent $\frac{1}{\gamma\beta} \in]1, \infty[$ takes value from 1, in the limit where $\mu \approx d + \beta$ while keeping $\beta \approx 1$ and ∞ when $\beta \to 0$. The model is limited by ℓ_0 and exponent that would lead to a faster growth than ℓ_0 should not be part considered.

To explore a range of values, we started from low μ and β to have high $\frac{1}{\gamma\beta}$ and went to higher μ and β, Fig. 9. Throughout the analysis of this scaling, one should always verify that the cost is limiting the growth. It can be done by analysing the leading and subleading contribution, both need to follow their asymptotical behaviour: $C(\ell(\tau)) \sim \tau$ and $\tau - C(\ell(\tau)) \sim \tau^{\gamma}$. Secondly ℓ_0 must be fast enough such that the cost can be limiting in time: $(\frac{1}{\mu-d} >> \frac{1}{\gamma\beta})$. Another issue makes the analysis harder in time: their is a simulation artefact. Indeed when the population is close to the final size, jumps that lands later in netcost might never contribute to the growth in time, slowing the growth. In other words, one needs to simulate bigger sizes than the one that can be analysed.

As we reach higher values of exponent $\frac{1}{\gamma\beta}$, we see how the simulated growth takes more time to approach the scaling. A problem might appear for $\frac{1}{\gamma\beta}$ high enough such that ℓ_0 has a similar scaling in that timescale. Therefore we need even longer simulations for the analysis of $\ell(t)$.

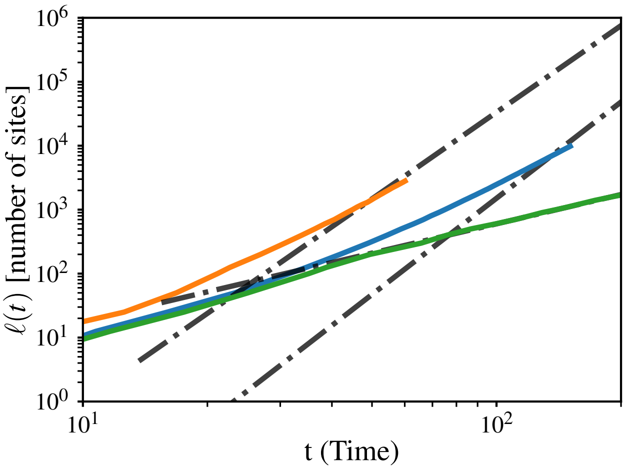

Figure 9: **Analysis of leading exponent in time**, orange: $\mu = 1$, $C(r) = 10r^{0.25}$, blue: $\mu = 0.8$, $C(r) = 100r^{0.25}$ and green: $\mu = 1.3$, $C(r) = 10r^{0.8}$. The black dashed curves are the expected fit scaling $\frac{1}{\gamma\beta}$ for the respective coloured curve. All the curves have been verified to scale as $\sim \tau^{\frac{1}{\beta}}$ in netcost

The numerical results are scarce due to the problems mentioned above. We cannot confirmed the theoretical derivations but the numerical results qualitatively follow the expectations. More investigations should be pushed in that direction with the mean of more computational resources.

4.2 Tree

To derive the behaviour with cost, we will assume that the bare growth is known and has the following form:

$$\ell_0(s) = \begin{cases} c_1 s, & \text{if } \ d < \mu < d+1 \\ c_1 s^{c_2}, & \text{if } \ \mu = d \\ c_1 s \exp(c_2 B_\mu s^{\eta}), & \text{if } \ \mu < d \end{cases} \tag{23}$$

Where c_1 and c_2 are fitted values. For $\mu < d$ the result can be derive using Eq. 26 and the same technics presented in section 2.3. In the following analysis the regime $\mu > d$ has not been analyzed further.

We aime at finding routes that minimizes the number of steps on the way together with additional costs that depends on the link distance; i.e. paths that minimzes the sum $\mathcal{T} = \sum_{i=1}^{N} Ar_i^{\beta} + N\delta$ for some amplitude δ. It is equivalent to consider cost of the form $C(r) = Ar^{\beta} + \delta$ for each link. If one wants to compare the results to ℓ_0, δ should be set to 1 such that a direct relation between the number of steps and the cost of a path can be made. But in the following we will not constraint ourselves to $\delta = 1$ but the growth in steps will always be counted by steps of size 1.

We recall briefly the algorithm: we built a Tree "on the fly" by choosing the outgoing link with minimum weight (from the source) leaving the nodes currently in the population. The resulting output was a shortest path Tree with the first node picked being the root.

4.2.1 Convex Cost

Considering $\beta \geqslant 1$ and $\delta = 1$, brings us in a setting similar to section 4.1.1. We add the number of steps on the path to the cost as we previously added the waiting times. The argument pictured in Fig. 3 is still valid for $\mu \leqslant 1$ and the speed can be calculated in the similar fashion. We calculate t^* through $C(\ell_0(t^*)) = t^*$ using Eq. 23 and then insert it in Eq. 17. The simplified behaviour we expected was a non-continuous change at s^* from $\ell_0(s)$ to $v_s s$. It leads to a speed $v_s = \ell_0(s^*)/s^*$, Eq. 15.

The fitted values are plotted on Fig. 10 with the expected rescaled speed. They match perfectly as long as $\ell_0(t^*) << \ell_0(T)$. As discussed in section 4.1.1, when the cost is low t^* increases and $\ell_0(t^*)$ can reach very high values. In such cases the simulation cannot follow and the deviations in Fig. 10b are simply linear fits on curves not linear yet. Similarly to the outbreak, high values of A have not been analysed here as they fall into the case depending on the specificity of the lattice. Assuming that links to neighbours always happen, we discuss the results in section A.4.

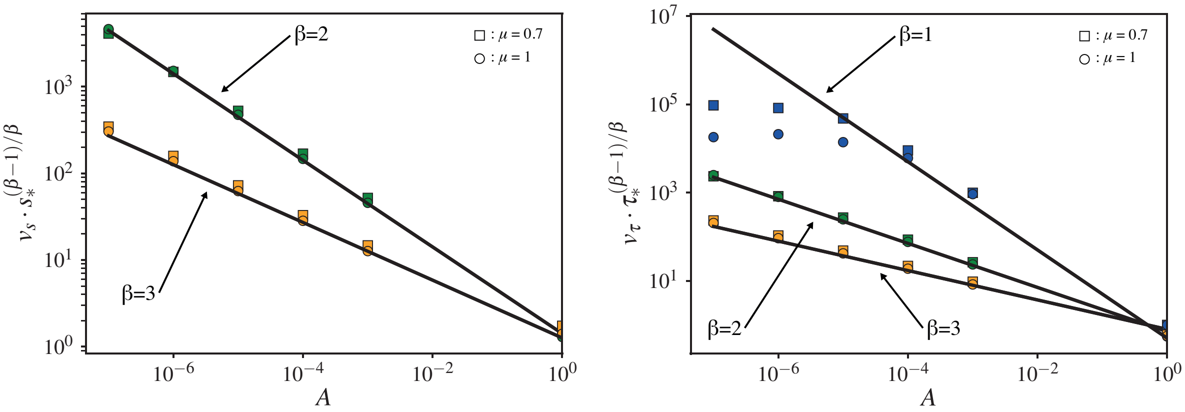

(a) Growth in steps

(b) Growth in netcost

Figure 10: **Rescaled speed for Tree simulations with** $k = 8$, using $\delta = 1$ and an average of five simulations of size $\ell(T) = 10^6$ for each geometric form. We used green for $\beta = 2$, yellow for $\beta = 3$ and blue for $\beta = 1$.

If $\delta = 0$ we loose the possibility of following the bare growth and increasing the final velocity. In this scenario, small links are always favourable compared to longer links leading to an unconditional linear growth. In order to see transient states appear the system needs to be set in a position where the Ar^{β} is negligible compared to δ. We showed how reducing A affects the speed. We now investigate how increasing δ influences the growth.

It is possible to tune δ to make longer links more favourable as well. Higher values of δ will penalise the successive short links and long ones will become advantageous once again [13]. In fact, as long as the length of the link r, respects: $Ar_{max}^{\beta} + \delta \leqslant r_{max}(A + \delta)$ direct links will have a smaller weight than a series of one step jumps. However this is the extreme situation, before that another phenomena will constraint the growth. Series of different sizes jumps will outcompete a direct link. For example, 2 links of size k will become more advantageous than one of $2k$. This phenomena will appear roughly when $Ar_{min}^{\beta} \approx 2\delta$. It will be possible to decompose a single link of length r_{min} into 2 smaller ones, Fig 11.

We propose a way to calculate the speed using the new limits on r that we found. First up to r_{min} every links are accepted: the cost is dominated by δ and long links are always better. The regime should act as ℓ_0. After r_{min} the length will be slowly limited to a series of smaller links. We see that starting from $r_{min} + 1$ one long jump to r_{min} and another one step to $r_{min} + 1$ is cheaper than paying a direct link. After a couple r_{min}, the system settles in a linear growth with a combination of links smaller than r_{min}. We set this number to 4 times r_{min} which matches well the simulations, Fig. 11. This number should be used with caution, different regimes can have slightly different values. Over the different forms we see that is scales as 3.5 ± 1.0.

$$4 \cdot r_{min} \approx \ell_0(s^*) \tag{24}$$

From this relation we can extract $\ell_0(s^*)$ and s^* and derive the speed $v_s = \ell_0(s^*)/s^*$.

In netcost the mechanism is different, already for the first step, the links paid is $\approx \delta$ which shifts the curve from ℓ_0 by δ in time. Long jumps are still more advantageous and the growth can follow a similar trend to ℓ_0 at a shifted time. Algorithmically speaking, the nodes reached are the same, however instead of counting the number of nodes accessible in s steps, we now count them after a cost τ. As $\delta >> A1^{\beta}$, the link price dominates the cost for length-one links. We conclude that the number of nodes reached at a cost $\tau = s \cdot \delta$ is given by $\ell(\tau^*) \approx \ell(s^*)$.

$$v_{\tau} = \frac{\ell(\tau^*)}{\tau^*} = \frac{\ell(s^*)}{s^*\delta} \tag{25}$$

We can go further and express the rescaled speed we expect for any μ: $v_{\tau}s^* = \frac{4r_{min}}{\delta}$. We plot the results on Fig. 12. When dealing with $\beta = 1$, the speed v_{τ} becomes δ independent, changing δ changes only the point where $\ell(\tau)$ meets this constant speed curve. The extra nodes contributing to the speed by the extension of r_{min} are fully compensate by the extra time they have to travel by increasing δ. However $\ell(s)$ never becomes linear (see next section), it does not intersect ℓ_0. In that case s^* does not hold any significance, it is set to 1, and Equ. 25 becomes:

$$v_{\tau}|_{\beta=1} = \frac{\ell(\tau^*)}{s^*\delta} = \frac{\frac{2\delta}{A}}{1\delta} \sim \frac{1}{A}$$

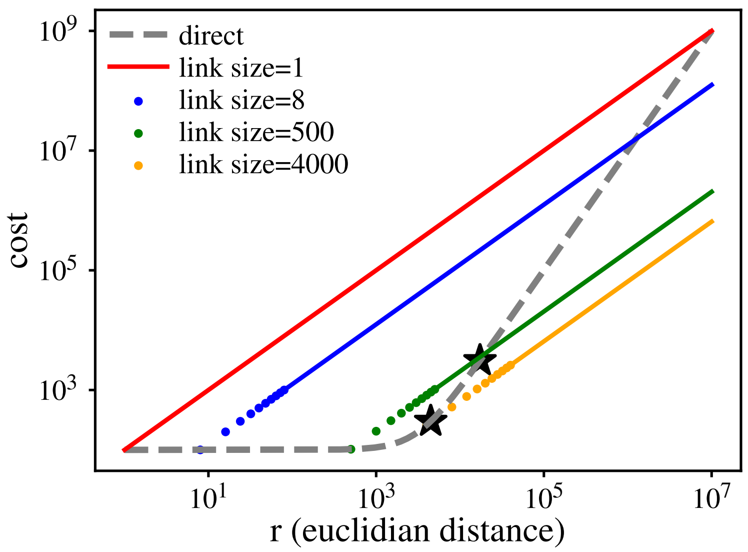

Figure 11: $C(r) = 10^{-5}r^2 + 100$, **Comparison of different link sizes as an optimal path**: The bottom star represents r_{min}. The second star correspond to $\ell(t^*_{\text{simulation}})$ for the same cost and $\mu = 0.7$. Here $\ell(t^*_{\text{simulation}}) \approx 4r_{min}$.

The only condition to see that scaling appear is to have A high enough such that $\ell(\tau^*) >> \ell(\mathcal{T})$. Further explanations of the speed for the case $\beta = 1$ are given in the next section, where we also expect a speed of $\frac{1}{A}$.

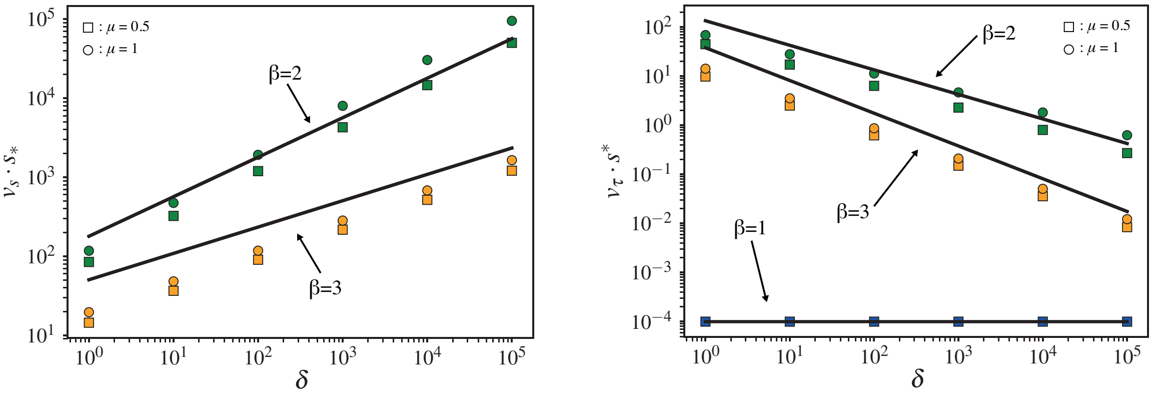

(a) Rescaled speed in steps, s. The black curves follow the form: $\sim 4(\frac{2\delta}{A})^{1/\beta}$

(b) Rescaled speed in netcost, τ. The black curves follow the form: $\sim \frac{4}{\delta}(\frac{2\delta}{A})^{1/\beta}$

Figure 12: **Rescaled speed for Tree simulations with** $k = 8$ and $C(r) = 1e^{-3}r^\beta + \delta$. Each geometric form is an average of five simulations of size $\ell(T) = 10^6$. We used green for $\beta = 2$, yellow for $\beta = 3$ and blue for $\beta = 1$.

Overall, we have a good description for the different restrictions leading to a linear growth. For low values of δ the crossover tends to happens faster than predicted by Eq. 24. When δ is close to one, one should prefer the approach $C(\ell_0(t^*)) = t^*$ which encompasses the μ dependance.

4.2.2 Concave Cost

The analysis for the system in netcost τ is qualitatively the same presented in section 4.1.2. The key jump are limited by the cost function which leads to a grow $\sim \tau^{1/\beta}$. Once again we set ourselves in a regime where the cost dominates the grows using A sufficiently high. The value of A is determined relatively to the value of δ. We are interested in a regime where the ratio $\frac{A}{\delta}$ is sufficiently high to observe the asymptotical behaviour $\sim \tau^{1/\beta}$. Setting δ to 1, we allow the transient phase to appear as well as asymptotical behaviour, Fig. 13. We note that when $\delta \to 0$, all values of A lead to the form $\sim \tau^{\frac{1}{\beta}}$.

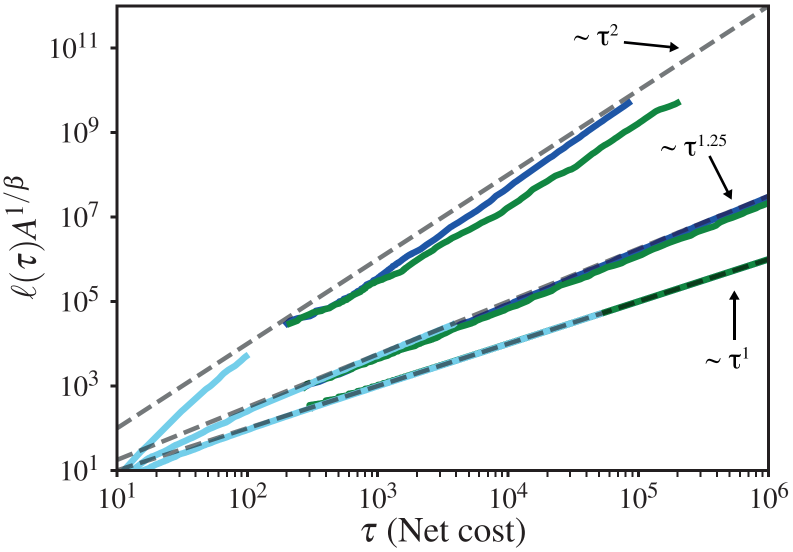

Figure 13: **Rescaled growth for various concave cost and μ, $k = 8$.** The grey dashed lines represent the asymptotical growth expected for the three β used with a constant speed. All $\ell(\tau)$ have been multiplied by $A^{1/\beta}$ which correspond to the inverse speed of the growth in those cases. For each β we plotted two values of μ: green are for $\mu = 1$ and $A = 1e^2$, blue and lightblue are for $\mu = 0.4$, $A = 100$ and $A = 0.1$ respectively. All coloured lines are average over 4 simulations of sizes 10^6.

In order to be able to restrict the growth, we need it to be faster than the limitation we impose, $\ell(\tau) \sim \tau^{1/\beta}$. For $\mu = d$ it means: $c_2 > \frac{1}{\beta}$, and all $\beta > 0$ when $\mu \leq d$, Eq. 23. On Fig. 13, we see that we $\frac{1}{\beta}$ gets closer to $c_2 \approx 3.4$, the speed slightly deviates from the expected one. For such cases, longer simulations are needed to give more possibilities to the maximum jumps allowed to occur. We also plotted lower values of A for the same parameters (red and blue curves), we see that when A is too low, the cost is not limiting and curve does not collapse on the expected one. We can also note that as β grows, smaller A is need to reach the asymptotical from.

We simulated spreading with different values of μ, β, k and A, and the results were in agreement with the predicted behaviour, as long we used a sufficiently high ratio $\frac{A}{\delta}$. In those cases we observed, for very different ℓ_0 (changing μ and k), the same collapse to $\ell(\tau) = A^{-1/\beta}\tau^{\frac{1}{\beta}}$.

Focusing on the growth in steps, we look at the saddle point approximation that was used to derive $\ell(S)$ for the Tree: Eq. 43 and we apply a similar reasoning to section 4.1.2. Eq. 43 is reduced to:

$$G[\ell(\mathcal{T})]\ell^{2d}\left(\frac{\mathcal{T}-A\ell^{\beta}(\mathcal{T})}{2}\right)\kappa_{\text{out}} \sim 1. \tag{26}$$

Assuming $\frac{\mathcal{T}-A\ell^{\beta}(\mathcal{T})}{2} \sim \tau$ and replacing in Eq. 26, we find that $\tau^{d+\mu} \sim \tau^{2d}$ leading to $\mu = d$. Something more is needed to analyse the case $\mu < d$. If we add another subleading term: $A\ell^{\beta} \sim \tau - \tau^{\lambda}$ we find that $\tau^{d+\mu} \sim \tau^{\lambda(2d)}$:

$$\lambda = \frac{d+\mu}{2d} \tag{27}$$

We analyse the sub-leading terms with the purpose of validating when a cost is limiting Fig. 14. As μ gets closer to 1 the sub-leading scaling gets closer to linear and the distinction between the two curves takes more time. Smaller μ make $\ell(\tau)$ grow faster hence the cost, which lead to a faster distinction between the blue and green curve.

Here we do not have waiting times, k destinations are chosen randomly and are only one step away from the source. We can not give an upper bound on $\ell(s)$ in a similar way. We propose the following approximation to analyse the scaling of the growth in **steps**.

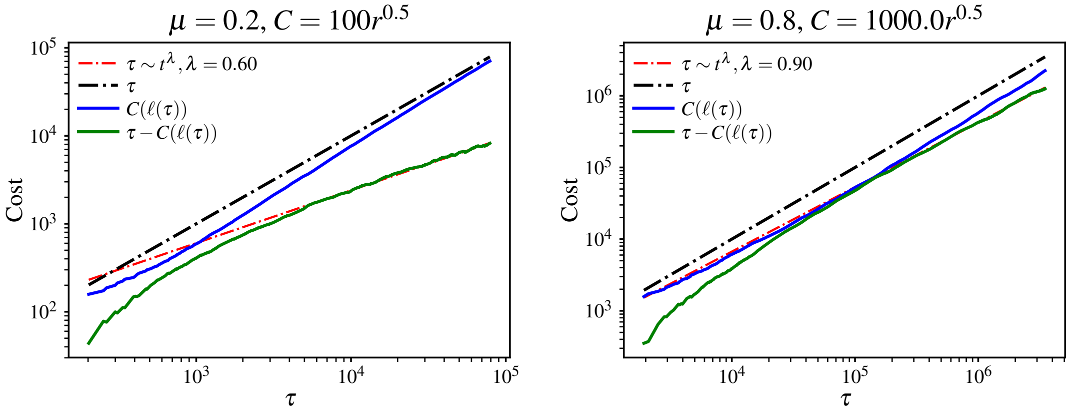

Figure 14: **Leading and subleading contributions to net cost**, from simulations (solid lines) compared to power-law predictions (broken lines). The prediction for δ is given in Eq. 27. The plot are average of 4 simulations of size 10^6 for the left panel and 10^7 for the right panel.

Using a **concave cost** slightly changes the sequences of chosen jumps to promote minimum path and changes the overall dynamic. To be able to speak about long jump we only consider $\mu \leqslant 1$. Indeed long jumps will happen with the same probability (compare toℓ_0) but now will be accepted in a later "stage". During that time the network will be filled with smaller jumps which total cost is cheaper since closer to the core. The question is when does a long jump enter in the competition? For example when we start with a jump to $r = 10^6$ with a cost of $C(r) = 1r^{0.5}$, $C(10^6) = 10^3$, the one-size jumps will be cheaper up to a radius of 10^3. In other word, we see that now the key jumps are not optimal from the beginning and a key jump of distance r has will see a core of r^{β} being filled. Does it change the growth? We can imagine that for low value of β it has a minimal impact and that the picture is similar to the one in the bare growth. However as β grows we will have less and less contribution from seeded clusters and the behaviour changes.

The expected growth in steps is thus slowed down by the cost. At a size $\ell(S)$ the iterative key jump argument is valid only after $\ell^{\beta}(S)$ has been filled and this repeat iteratively (key jump in $\ell^{\beta}(S)$, $\ell^{\beta^2}(S)$ must be filled).

We start by analysing how the growth is modified, Fig. 15. The fit minimising the mean square error found for the limited curves scales as: $\ell(s) \sim s^{c_2-\beta}$. We observed this scaling for a wide range of $k > 4$. We make the following conclusions: while the growth wants to follow $\ell_0(s)$, s^{β} steps are required for the key jump to occur.

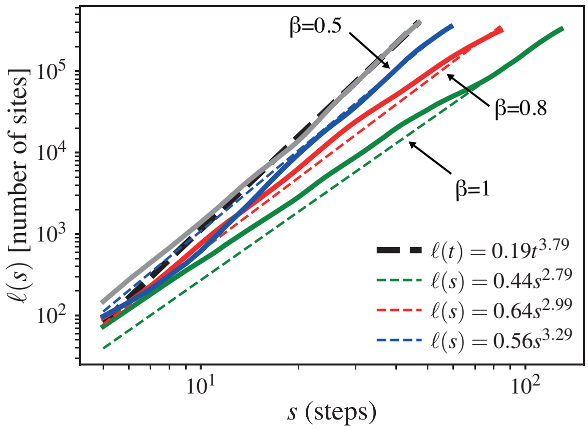

Figure 15: **Tree spreading for** $\mu = 1$ **and** $C(r) = 100r^{\beta} + 1$ **,** $k_{out} = 12$. Plotted curves are averaged over 4 simulations of size $\ell(S) = 5 \cdot 10^5$.

We analyse how this rescaling affects lower values of μ, Fig. 16. As μ is reduced and spatial concerns become less relevant, the scaling gets poorer and poorer. Overall this approximation gives a good intuition on the scaling but lack the power of quantifying the speed which influences greatly the spread. It should still be considered as an exploratory result and further investigations should be push in that direction.

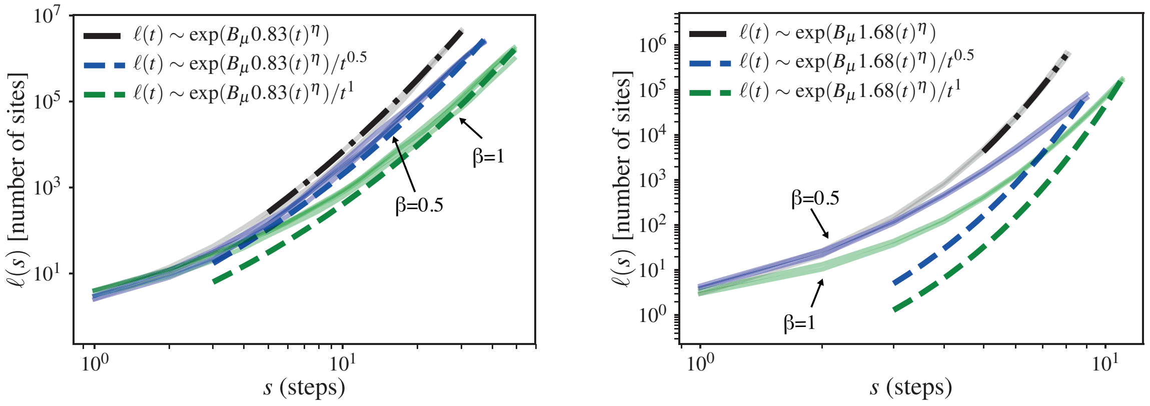

(a) $\mu = 0.7, A = 100, k = 12$: blue: $\beta = 1$, orange: $\beta = 0.5$

(b) $\mu = 0.2, A = 100, k = 12$: green: $\beta = 1$, blue: $\beta = 0.5$

Figure 16: **Concave growth Tree** $\mu < 1$ with cost in color $C(r) = Ar^{\beta} + 1$. Plotted curves are averaged over 4 simulations of size $\ell(S) = 10^6$

5 Conclusion

We showed what form to expect for ℓ when the cost is restricting. But for a finite time, there is a continuum of transient states that ℓ can take, from ℓ_0 to $\ell_{\text{restricted}}$. Understanding evolution under some restrictions passes by knowing when does the constraints become relevant. We saw that finding this time point is not trivial in every cases, and that the behaviour might change but not as strongly as expected for a relatively long period of time. For both models, we saw that under some convex cost any type of growth becomes linear at some point and the only dependance to μ becomes finding that point.

Convex cost impacts on the growth have been well understood and the resulting form can be entirely predicts, knowing the initial spreading and the limitations applied on it. The resulting expansion under a concave cost could not be fully apprehended, mainly because the point where the asymptotical behaviour appears is not as clear. However once we reached this regime, the growth in netcost can be completely derived analytically. We showed that in that case, the restrictions leave little space for the initial behaviour to influence the final growth.

In a broader framework, the netcost analysis can be interpreted in two ways. The Outbreak model can be mapped to a problem of first-passage percolation [27, 28]. Concerning the Tree algorithm, [29] showed that using shortest paths as a source of length scales helps to explore the fractality of networks.

The most relevant model for transportation and human interactions is the Tree. δ can model the base cost people are willing to pay and easily tunes the models while the power-law can fit different modes of transportation or communication. Further work can be done comparing the Tree to shortest path on networks with a strong coupling to the underlying geometry [29, 30]. The algorithm also prepared the framework for scale-free degree distribution where we expect quantitative changes [31]. On a computational side, the algorithm revealed itself to be fast and not as memory expensive as the Outbreak can be. When the usage of the STL library becomes limiting, one should think about using their own containers.

We expect our approach to be particularly useful for solving optimisation problems on network. Its potential of giving the nodes or space reachable within a certain time and/or cost makes it useful for practical interest. It gives us intuition about a number of situations such as the design of transportation systems, parcel delivery services or contagious diffusion.

References

[1] D. Fisher, M. Lässig, and B. Shraiman, “Evolutionary dynamics and statistical physics,” *Journal of Statistical Mechanics: Theory and Experiment*, vol. 2013, no. 1, pp. 1–8, 2013.

[2] O. Hallatschek and D. S. Fisher, “The acceleration of evolutionary spread by long-range dispersal,” 2014.

[3] G. S. Jacobs and T. J. Sluckin, “Long-range dispersal, stochasticity and the broken accelerating wave of advance,” *Theoretical Population Biology*, vol. 100, 2015.

[4] P. G. Higgs, “Frequency distributions in population genetics parallel those in statistical physics,” vol. 51, no. 1, 1995.

[5] R. A. Fisher, “The wave of advance of advantageous genes,” *Ann. Eugenics*, vol. 7, pp. 353–369, 1937.

[6] I. G. P. A. N. Kolmogorov and N. S. Piscounov, “Étude de l’équation de la diffusion avec croissance de la quantité de matière et son application à un problème biologique,” *Bull. de l’Univ d’état à Moscou (ser. intern.)*, vol. Sec. A, pp. 1–25, 1937.

[7] P. Ralph and G. Coop, “Parallel adaptation: One or many waves of advance of an advantageous allele?,” *Genetics*, vol. 186, no. 2, pp. 647–668, 2010.

[8] D. Taylor, F. Klimm, H. A. Harrington, M. Kramár, K. Mischaikow, M. A. Porter, and P. J. Mucha, “Topological data analysis of contagion maps for examining spreading processes on networks,” *Nature Communications*, vol. 6, 2015.

[9] D. J. Watts and S. H. Strogatz, “Collective dynamics of ’small-world’ networks,” *Nature*, vol. 393, no. 6684, pp. 440–442, 1998.

[10] R. Guimera, S. Mossa, A. Turtschi, and L. A. N. Amaral, “The worldwide air transportation network: Anomalous centrality, community structure, and cities’ global roles,” no. Track II, 2003.

[11] T. Verma, N. A. M. Araújo, and H. J. Herrmann, “Revealing the structure of the world airline network,” *Scientific Reports*, vol. 4, pp. 1–6, 2014.

[12] G. Burghouwt, J. Hakfoort, and J. R. van Eck, “The spatial configuration of airline networks in Europe,” *Journal of Air Transport Management*, vol. 9, no. 5, pp. 309–323, 2003.

[13] M. T. Gastner and M. E. J. Newman, “Optimal design of spatial distribution networks,” pp. 2–7, 2006.

[14] N. Shigesada and K. Kawasaki, *Biological invasions: theory and practice.* 1997.

[15] S. Milgram, “The small world problem,” *Psychology today*, vol. 2, no. 1, pp. 61–67, 1967.

[16] R. Pastor-Satorras, C. Castellano, P. V. Mieghem, and A. Vespignani, "Epidemic processes in complex networks," *Working paper*, pp. 1–62, 2015.

[17] P. Grassberger, "SIR epidemics with long-range infection in one dimension," *Journal of Statistical Mechanics: Theory and Experiment*, vol. 2013, p. P04004, apr 2013.

[18] P. Grassberger, "Two-Dimensional SIR Epidemics with Long Range Infection," *Journal of Statistical Physics*, vol. 153, pp. 289–311, oct 2013.

[19] M. Biskup, "On the scaling of the chemical distance in long-range percolation models," *Annals of Probability*, vol. 32, no. 4, pp. 2938–2977, 2004.

[20] D. Bonte, Van Dyck, *et al.*, "Costs of dispersal," *Biological Reviews*, vol. 87, no. 2, pp. 290–312, 2012.

[21] S. R. Jara Díaz, "The estimation of transport cost functions: A methodological review: Foreign summaries," *Transport Reviews*, vol. 2, no. 3, pp. 257–278, 1982.

[22] T. Garland, "Scaling the Ecological Cost of Transport to Body Mass in Terrestrial Mammals," *The American Naturalist*, vol. 121, no. 4, pp. 571–587, 2018.

[23] S. E. Grønland, "Cost models for transportation and logistics," no. 0349, 2014.

[24] C. P. Robert and G. Casella, *Random Variable Generation*, pp. 35–70. New York, NY: Springer New York, 1999.

[25] D. R. Tobergte and S. Curtis, *Effective STL: 50 Specific Ways to Improve Your Use of the Standard Template Library*, vol. 53. 2013.

[26] E. W. Dijkstra, "A note on two problems in connexion with graphs," *Numerische Mathematik*, vol. 1, no. 1, pp. 269–271, 1959.

[27] S. Roux, A. Hansen, and E. L. Hinrichsen, "A direct mapping between Eden growth model and directed polymers in random media," *Journal of Physics A: Mathematical and General*, vol. 24, pp. L295–L300, mar 1991.

[28] X. Cao, A. Rosso, J.-P. Bouchaud, and P. Le Doussal, "Genuine localization transition in a long-range hopping model," *Physical Review E*, vol. 95, p. 062118, jun 2017.

[29] G. García-Pérez, M. Boguñá, and M. Á. Serrano, "Multiscale unfolding of real networks by geometric renormalization," 2017.

[30] K. Bringmann, R. Keusch, and J. Lengler, "Average Distance in a General Class of Scale-Free Networks with Underlying Geometry," 2016.

[31] M. Boguñá and D. Krioukov, "Navigating ultrasmall worlds in ultrashort time," *Physical Review Letters*, vol. 102, no. 5, pp. 1–4, 2009.

[32] S. A. O. Carl M. Bender, *Advanced Mathematical Methods for Scientists and Engineers.*

A Calculus

A.1 Logistic Growth

Inside a deme we suppose logistic growth, both for the wild type as well as the mutant:

- The wild population p :
$$\frac{dp}{dt} = \alpha p \frac{\hat{n} - p}{\hat{n}} \tag{28}$$
- The population with mutation p_{mut} :
$$\frac{dp_{mut}}{dt} = \alpha(1+s)p_{mut}\frac{\hat{n} - p_{mut}}{\hat{n}} \tag{29}$$

The solution of the differential Eq. 28 is of the form

$$p(t) = \frac{\hat{n}p_0 e^{\alpha t}}{\hat{n} + p_0(e^{\alpha t} - 1)} \tag{30}$$

here p_0 is the initial density of individuals and α the growth rate for the population.
In logistic growth, a population's growth rate gets smaller and smaller as population size approaches a maximum imposed by limited resources in the environment, limiting the density to $\hat{n}$.

A.2 Iterative scaling argument

We start from Eq. 9:

$$tG[\ell(T)]\ell\left(\frac{T}{2}\right)^{2d} \sim 1 \tag{31}$$

Taking the log of the expression leads to a general first order inhomogeneous linear difference equation:

$$\log_2(t) + \log_2(G(\ell(T))) + 2d\log(\ell(\frac{T}{2})) = 0 \tag{32}$$

Applying a change of variable : $\log_2(t) = z$, $\log_2(\ell(t)) = \phi(z)$

$$z + 2d\phi(z-1) = (d+\mu)\phi(z) \tag{33}$$

Formally we have:

$$\phi(z+1) = (\frac{2d}{d+\mu})\phi(z) + \frac{z+1}{d+\mu} \tag{34}$$

which has a solution [32] (multiplying both sides by a summing factor and summing both sides) of the form:

$$\phi(z) = (\frac{2d}{d+\mu})^{z-1}\left[\sum_{k=0}^{z-1}\frac{\frac{k+1}{d+\mu}}{\prod_{j=1}^{k}\frac{2d}{d+\mu}} + \phi(0)\right] \tag{35}$$

using $p = \frac{2d}{d+\mu}$

$$\begin{aligned} \phi(z) &= p^{z-1} \cdot [p^{1-z} \tfrac{1}{d+\mu} \tfrac{p^{z+1}-p(z+1)+z}{(p-1)^2}] \\ &= \tfrac{p^z + z(\frac{1-p}{p})-1}{\frac{(d-\mu)^2}{2d}} \\ &= \tfrac{2d}{(\mu-d)^2} p^z + \tfrac{z}{\mu-d} - \tfrac{2d}{(\mu-d)^2} \end{aligned} \tag{36}$$

- When $d < \mu < d+1$ the first term of Eq. 10 dominates at large z:

$$\phi(z) \approx \frac{z}{\mu - d} - \frac{2d}{(\mu - d)^2} \tag{37}$$

$$\begin{aligned} \ell(t) &\approx 2^{(\frac{\log_2(t)}{\mu-d} - \frac{2d}{(\mu-d)^2})} \\ &= 2^{-\frac{2d}{(\mu-d)^2}} \cdot t^{\frac{1}{\mu-d}} \end{aligned} \tag{38}$$

- When $\mu < d$ the second term dominates at large z due to the exponential growth:

$$\log_2(\ell(t)) \approx \frac{2d}{\mu - d}^2 (\frac{2d}{\mu + d})^{\log_2(t)} \tag{39}$$

$$\ell(t) = \exp(\frac{2d\log(2)}{(\mu - d)^2} t^{\log_2(\frac{2d}{\mu+d})}) \tag{40}$$

- When $\mu = d$ both therms needs to be accounted, furthermore we can show that the result: $\ell(t) \sim \exp(\frac{\log^2(t)}{4d\log(2)})$ is valid not only for asymptotic behaviour but also intermediate regime.

A.3 Scaling on fixed network

The growth on the network is similar to the outbreak case. However due to the fixed number of links out of a node, it will resume by having only the key jumps starting from the border of the core funnel.

$$\int_0^S ds \int_{\text{border}} d^d\mathbf{x} \int_{\text{target}} d^d\mathbf{y}\, G(|\ell(S)\mathbf{e} + \mathbf{y} - \ell(s)\mathbf{e}|) \sim 1, \tag{41}$$

We still consider $\mathbf{y}$ and $\ell(s)$ negligible compared to $\ell(S)$, leading to the same type of integral:

$$G[\ell(S)] \int_0^S dt\, \ell^d(s)\ell^d(S - s) \sim 1. \tag{42}$$

Now the steps integral do not lead to a s indeed each sites can send only k_{out} links independently of s.

$$G[\ell(S)]\ell\left(\frac{S}{2}\right)^{2d} k_{\text{out}} \sim 1. \tag{43}$$

A.4 Lattice dependent speed

The expansion of the infected sites in the case where $\beta \geqslant 1$, can be such that only the last site contributes. This phenomenon appears when the cost associated to the jumps is dominating the waiting times to pick the sites, even for jumps of size 1. In such cases, the difference of cost between a jump of size 2 and size 1, is bigger than the average time required to pick the site allowing a jump of size 1. It can be mathematically formulated as follows:

$$A2^{\beta} - A > W_1 \tag{44}$$

where we define W_i as the average waiting time to pick site i, $\mathbb{P}(j_i)$ is the probability per unit of time to make a jump of length i. Every timestep dt there is a probability $\frac{1}{N}$ to pick the last site. On average, after one unit of time, the probability to pick that site and jump to the nearby site is given by :

$$\mathbb{P}(j_i) = \frac{1}{2} \int_{i}^{i+1} \frac{\mu + d - 1}{r^{\mu+d}} dr \approx \frac{1}{W_i} \tag{45}$$

In that case the two speeds are simply given by $v_{\mathcal{T}} = \frac{1}{A+W_1}$ and $v_t = \frac{1}{W_1}$.

The same derivation can be done for the Tree model where W_1 is replaced by δ. The resulting speeds are: $v_{\mathcal{T}} = \frac{1}{A+\delta}$ and $v_s = \frac{1}{\delta}$.